This is a preprint version of the article published in the

Journal of Aerosol Science, 37, 786-798 (2006)

FIELD MEASUREMENTS AND SIZE-RESOLVED MODEL SIMULATIONS OF TURBULENT PARTICLE TRANSPORT TO A FOREST CANOPY

Andreas Held[1,*], Andreas Nowak[2], Alfred Wiedensohler[2], and Otto Klemm[1]

[1] Bayreuth Institute of Terrestrial Ecosystem Research (BITÖK), University of Bayreuth, D-95440 Bayreuth, Germany

Now at: Institute of Landscape Ecology (ILÖK), University of Münster, D-48149 Münster, Germany

[2]Institute for Tropospheric Research (IfT), D-04318 Leipzig, Germany

RUNNING TITLE: SIZE-RESOLVED TURBULENT PARTICLE TRANSPORT

[*] Corresponding author:

Phone: +49-251-83-33923

Fax: +49-251-83-38352

andreas.held@uni-muenster.de (A. Held)

ABSTRACT

Direct measurements of turbulent particle number fluxes above a Norway spruce forest are compared with a size-resolved particle deposition model in combination with particle size distribution measurements. In most cases, the model output is in reasonable agreement with the eddy covariance measurements. The combination of deposition model and size distribution measurements allows the evaluation of size-resolved particle number and mass fluxes. While turbulent particle number fluxes are dominated by ultrafine particles below 50 nm diameter, submicron particle mass fluxes are established mainly in the accumulation mode. The effective deposition diameter D_{ed} is introduced as a new parameter to describe the effect of the size distribution of a polydisperse particle population on the integral particle transfer velocity.

KEYWORDS

turbulent particle number flux, particle mass flux, particle deposition model, particle size distribution, effective deposition diameter

1 INTRODUCTION

The atmospheric aerosol is a highly dynamic system that affects our lives in multiple ways: Atmospheric particles play a key role in the global radiation budget and climate (e.g. Schwartz, 1996). Also, many aspects of atmospheric chemistry are affected by the presence of particulate matter, e.g. stratospheric ozone depletion and the tropospheric ozone budget (Seinfeld and Pandis, 1998). Recently, adverse health effects of high atmospheric particle loadings have been in the focus of scientific interest (e.g. Wallace, 2000).

Most effects of the atmospheric aerosol are strongly dependent on particle size. Therefore, it is essential to study size-dependent transport mechanisms such as the turbulent particle deposition behavior controlling the atmospheric distribution / redistribution of particles and the corresponding atmospheric residence times. Quantification of these processes is a challenging task. The direct measurement of turbulent particle fluxes has recently been a field of intense research efforts and various approaches exist. However, current measuring instrumentation is limited in its ability to provide size-resolved particle number and mass fluxes. In most cases, size-dependent deposition behavior of particles is modeled while models have not been evaluated systematically through direct atmospheric measurements. Thus, many uncertainties complicate the quantification of particulate input to, and export from, ecosystems (Wesely and Hicks, 2000). In particular, the direct quantification of turbulent exchange of ultrafine particles with diameters smaller than 100 nm is still an unresolved challenge (Buzorius *et al.*, 2003).

In this study, direct eddy covariance measurements of turbulent particle number fluxes are compared with results obtained from the combination of a size-resolved particle deposition model and size distribution measurements. The combination of deposition model output and size distribution measurements is also used to estimate submicron particle mass fluxes and to evaluate the flux contribution of different particle size fractions. Finally, the so-called

effective deposition diameter is introduced. Information about the size distribution of a particle population is condensed in this single parameter. We consider the combination of deposition models and direct eddy covariance measurements in this work an important contribution to submicron particle deposition studies.

2 METHODS

2.1 Site and measurements

Eddy covariance particle flux measurements were carried out in July/August 2001 and 2002 within the BEWA field campaigns of the German atmospheric research program AFO2000 (Klemm *et al.*, 2005; Steinbrecher *et al.*, 2004) at the "Waldstein" ecosystem research site of the Bayreuth Institute of Terrestrial Ecosystem Research (BITÖK). This Norway spruce site is situated in the "Fichtelgebirge" mountain range near the Czech/German border (50°09'N, 11°52'E, 776 m asl). A more detailed description of the site is given in Matzner (2004).

The eddy covariance particle flux system combined a Young Model 81000 sonic anemometer (R.M.Young, Traverse City, MI, USA) and two condensation particle counters: a CPC 3760A (CPC) and a UCPC 3025 (UCPC; both TSI Inc., St. Paul, MN, USA). The 50 % lower detection limit of the CPC was approximately at 11 nm diameter, the 50 % detection limit of the UCPC at approximately 3 nm (TSI, 1989; TSI, 1998). A standard PC was used for system control, data acquisition and data storage. The sonic anemometer data were sampled with a time resolution of 10 Hz. Also, the CPC and UCPC data were fed into electronic counting boxes (elub 0661, Universität Bayreuth, Germany) with a fixed time resolution of 10 Hz. The sonic anemometer and the CPC were mounted on a swinging boom at 22 m agl on the SE corner of a 30 m scaffolding tower surrounded by Norway spruce (Picea abies (L.) Karst). All other parts of the eddy covariance system were located on the 21 m tower platform. Further details of this system are given in Held and Klemm (2005).

Particle size distributions were continuously measured using a twin differential mobility particle sizer (TDMPS; Birmili *et al.*, 1999) with a time resolution of 15 – 20 min. Particles were sampled through a PM10 inlet next to the eddy covariance system inlet at the same height. The setup consisting of two Vienna-type differential mobility analyzers (DMA) for size separation and two condensation particle counters (CPC 3010 and UCPC 3025, TSI Inc., St. Paul, MN, USA) covered a size range from 3 to 900 nm diameter in 2001 and 3 – 800 nm in 2002 with 40 size bins, respectively. Observations of particle formation and growth with this system are described in Held *et al.* (2004).

2.2 Deposition model

A wide variety of model approaches based on wind tunnel experiments or theoretical parameterizations of deposition mechanisms are used to estimate size-dependent transfer velocities of particles. Many particle deposition models are modifications of the approach described by Slinn (1982). However, large differences between models were found, particularly in the diameter range from 100 nm to 1000 nm (Ruijgrok *et al.*, 1995). Also, in comparison with measurements, most models underestimate particle deposition velocities.

In this study, the particle deposition model of Zhang et al. (2001) based on the Slinn (1982) approach was applied. This model considers the processes of turbulent transfer, Brownian diffusion, impaction, interception, gravitational settling, and particle rebound. All deposition processes are described using simplified empirical parameterizations that have been modified to give a better reproduction of experimental observations especially in the submicron range. Input parameters of the particle deposition model include the particle diameter D_p [m], the friction velocity u_* [m s^{-1}], the Obukhov length L [m], temperature T [K], and the mean horizontal wind velocity [m s^{-1}]. For each of the 40 size bins of the DMPS system, individual transfer velocities were calculated for 30 min intervals. The friction velocity and the Obukhov length were taken from the eddy covariance system, temperature and wind velocity from the

BITÖK routine measurements in 21 m agl. Additional model parameters are summarized in Tab. 1.

→ Tab. 1

Many of the empirical parameters are still poorly defined and thus frequently used to adjust models to fit field measurements. Due to the fact that ultrafine particles were taken into account in this study, the parameterization of Brownian diffusion is critical. Within reasonable limits, the parameterizations of impaction and interception have negligible influence on the model output in our study. Adjustment of the empirical diffusion parameter to $\gamma = 0.81$ led to improved agreement between field observations and model results (cf. Figs. 2 and 7).

Normalizing the particle flux by the particle concentration yields the so-called particle transfer velocity v_t [m s^{-1}]. It quantifies the surface-atmosphere exchange of aerosol particles and may be derived from direct measurements of the particle flux F [m^{-2} s^{-1}] and the particle concentration c [m^{-3}] through

$$v_t = -\frac{F}{c} \qquad \text{[Eq. 1].}$$

Because particle fluxes are established in both directions, the term “transfer velocity” is preferred over the widely used term “deposition velocity” suggesting a limitation to deposition of particles. The statistical uncertainty of the transfer velocity measurements due to the counting statistics of the particle counters was calculated acc. Buzorius *et al.* (2003). In this study, the v_t uncertainty reaches maximum values of 0.2 mm s^{-1} for the CPC 3760A and 1.0 mm s^{-1} for the UCPC 3025, respectively.

Depending on shape, structure and size, aerosol particles exhibit distinct transfer velocities in the atmosphere. Therefore, in order to quantify the particle number flux, both the particle size

distribution and the turbulent exchange behavior of distinct size fractions have to be taken into account. The particle deposition model acc. Zhang *et al.* (2001) was used to describe the size-resolved particle deposition while the particle size distribution was directly measured. In Fig. 1, exemplary 30-min data are shown for a DMPS measurement comprised of 40 size bins.

→ Fig. 1

2.3 Integral vs. size-resolved transfer velocities

A combination of modeled particle transfer velocities $v_{t,i}$ and the measured particle number concentrations c_i of size bin i yields the size-resolved particle flux F_i,

$$F_i = -v_{t,i} \cdot c_i \qquad \text{[Eq. 2].}$$

The total flux of a polydisperse particle population may be described as the sum of the fluxes of several quasi-monodisperse size fractions,

$$F = \sum_i -v_{t,i} \cdot c_i \qquad \text{[Eq. 3],}$$

with F, total flux of polydisperse particle population [m^{-2} s^{-1}], $v_{t,i}$, transfer velocity of size fraction i [m s^{-1}], c_i, particle concentration of size fraction i [m^{-3}].

When using condensation particle counters, particle fluxes and concentrations are measured over wide size ranges. Thus, the resulting transfer velocity has to be considered an integral parameter of a polydisperse particle population. The integral transfer velocity v_{total} of a particle counter with lower detection limit D_{min} and upper detection limit D_{max} may be defined as

$$v_{total} = \frac{\int_{D_{min}}^{D_{max}} v_t(D_p) \cdot N(D_p) dD_p}{\int_{D_{min}}^{D_{max}} N(D_p) dD_p} \qquad \text{[Eq. 4]},$$

with $v_t(D_p)$, transfer velocity at diameter D_p [m s^{-1}], $N(D_p)$, particle number concentration at diameter D_p [m^{-3}] (e.g. Buzorius et al., 2003). Acc. to Eq. 4, particle counters with different detection limits may yield different transfer velocities depending on the measured particle fraction. In order to compare particle exchange measurements and particle deposition models, the modeled size-dependent transfer velocities have to be weighted with the measured size distribution. For the DMPS system with 40 size bins, Eq. 4 was adapted to yield

$$v_{t,\mathrm{mod}} = \frac{\sum_{i=1}^{40} v_t(i) \cdot N(i)}{\sum_{i=1}^{40} N(i)} \qquad \text{[Eq. 5]},$$

with $v_{t,mod}$, modeled integral transfer velocity for the DMPS size range [m s^{-1}], $v_t(i)$, transfer velocity of the DMPS size bin i [m s^{-1}], and N(i), particle number concentration in DMPS size bin i [m^{-3}].

2.4 Mass fluxes

In order to derive particle mass distributions from particle number distributions, the following idealizations may be assumed: (1) the diameter of all particles of size bin i equals D_i, (2) all particles are spherical, and (3) the density of all particles equals ρ. Then, the particle volume V_i of each size bin i with N_i particles may be calculated from

$$V_i = N_i \cdot \frac{1}{6} \cdot \pi \cdot D_i^3 \qquad \text{[Eq. 6]},$$

and the particle mass m_i of each size bin i is given by

$$m_i = \rho \cdot V_i \qquad \text{[Eq. 7]}.$$

In this work, the particle density is set to ρ = 1.3 g cm^{-3} taking into account both the higher densities of inorganic particulate compounds and the lower densities of organic compounds or

water. Then, the approximate particle mass flux may be calculated for each size bin i in analogy to Eq. 2.

3 RESULTS AND DISCUSSION

3.1 Model performance

→ Fig. 2

Fig. 2 shows the measured integral transfer velocity of the UCPC system and the modeled transfer velocity integrated acc. to Eq. 5. While the model approach takes into account the size range from 3 to 800 nm diameter, the UCPC measurement covers the size range from 3 nm to ~ 3 µm. The lower size range limits are identical. The difference in the upper size range limit is expected to be negligible with regard to turbulent number fluxes due to the steep decrease in particle number concentration with increasing diameter. The patterns of the modeled and measured time series are very similar. For example, the double peak on 29 July 2002 can be observed in both the measurement and the model. Negative transfer velocities, i.e. particle emission such as in the morning of 30 July 2002, are not reproduced by the model due to the lack of emission mechanisms in the model. Adjusting the empirical diffusion coefficient to $\gamma = 0.81$ yields the closest fit to a 1:1 agreement between model results and measured data. The parameterization of particle collection by diffusion is three times larger in the model by Zhang et al. (2001) as compared to the original parameterization by Slinn (1982). Increasing the empirical diffusion coefficient decreases the deposition due to diffusion if the particle diffusivity is larger than the kinematic viscosity of air. This is always the case in our study. Thus, increasing the diffusion coefficient γ from 0.67 to 0.81 yields a lower contribution of diffusion to particle deposition. Also, the minimum of the size dependent

deposition velocity function is shifted to smaller particle sizes. This is in accordance with previously published data and parameterizations (e.g. Nemitz et al., 2002).

In general, the particle deposition model of Zhang *et al.* (2001) provides a reasonable estimate of the size-resolved particle number flux in the submicron size range. The agreement of all 608 flux measurements and the corresponding model results may be considered satisfying. The Spearman's coefficient of rank correlation is R_s = 0.67. Since the model appears to perform well and predicts the transfer velocities with reasonable agreement with measurements, we used it to calculate size-resolved particle number and mass fluxes as displayed in Fig. 3.

3.2 Size-resolved fluxes

→ Fig. 3

Fig. 3 represents typical conditions of strong particle deposition fluxes. The particle number flux (Fig. 3a) is dominated by particles in the size range from 5 to 30 nm diameter. The contribution of particles > 50 nm diameter to the number flux is negligible. In contrast, the particle mass flux (Fig. 3b) is dominated by accumulation mode particles. In this example, the mass fluxes of the 40 size bins result in a total particle mass flux of 5 ng m^{-2} s^{-1} for the size range from 3 to 800 nm. However, this size range constitutes only a fraction of the total particulate mass in the atmosphere.

It is remarkable to note that the contributions of different size fractions to particle number and particle mass fluxes vary considerably. A more thorough analysis may be performed with the cumulative normalized particle concentrations and fluxes as displayed for a typical deposition episode in Fig. 4

→ Fig. 4

The cumulative normalized particle concentration describes the number or mass fraction of particles below a given diameter. Analogously, the cumulative normalized particle flux describes the contribution of particles below a given diameter to the particle number or particle mass flux. Fig. 4 indicates that 95 % of the number flux was contributed by particles below 30 nm diameter whereas these particles constitute only about 5 % of the mass flux. Particle mass flux is dominated by larger particles: The size range from 30 to 400 nm contributes 90 % of the mass flux. In contrast, this size fraction contributes only 5 % of the total particle number flux. In a similar fashion with respect to particle concentration, the number concentration is dominated by ultrafine particles below 100 nm ∅, whereas the mass concentration is dominated by accumulation mode particles. Interestingly, the bimodal character of the particle number size distribution (open diamonds) is strongly reduced in the size distribution of the particle number flux (black diamonds).

Because the particle number concentration of coarse particles above 1 µm diameter is negligible compared to the number of nucleation and Aitken particles, the DMPS system covers the size range relevant for the particle number flux. However, a valid estimation of the turbulent exchange of particulate mass based on the particle number flux is hardly possible. The evaluation of the submicron size range ignores the turbulent exchange of coarse particles even though these particles contribute a significant fraction of the particulate mass.

3.3 Effective deposition diameter

In order to summarize the impact of the particle size distribution on turbulent transport in a single parameter, the concept of the so called effective deposition diameter D_{ed} will be developed. This parameter is derived from the measurement of particle number fluxes and the

particle deposition model with input of turbulence parameters (cf. section 2.2). Assumptions about the size distribution of the considered particle population are not made.

For a given time interval, the measured integral transfer velocity may be compared with theoretical transfer velocities for various particle diameters obtained from size-resolved deposition models. Generally, there will be two distinct particle diameters with modeled transfer velocities corresponding to the measured integral transfer velocity (cf. Fig. 5).

→ Fig. 5

The effective deposition diameter D_{ed} is defined as the smallest particle diameter D_p for which $v(D_p) = v_{total}$ is fulfilled. The selection of the smallest diameter by definition may appear somewhat arbitrary, however, it is motivated by the fact that the number of small particles in the nucleation and Aitken mode dominates over accumulation mode particle numbers, thus also dominating the integral transfer velocity.

In the following, the theoretical relevance of the effective deposition diameter will be illustrated: Within a polydisperse population of N particles with an integral transfer velocity v_t and a corresponding flux F, particles exhibit different deposition velocities depending mainly on particle size. If we consider a monodisperse population with the same number of particles N, the same integral transfer velocity v_t and the same flux F, all particles exhibit the same transfer velocity equal to the integral transfer velocity v_t, and the uniform particle diameter in this population corresponds to the effective deposition diameter D_{ed}. In other words, a polydisperse population may be transformed into a monodisperse population without changing the particle flux if all particle diameters are set to D_{ed}.

Particle populations dominated by nucleation mode particles tend to exhibit relatively small D_{ed} values, whereas aged populations with a pronounced accumulation range will have

considerably larger D_{ed} values. Thus, the effective deposition diameter combines information about the particle size distribution in a single parameter. This feature is illustrated in Fig. 6.

→ Fig. 6

Fig. 6 shows the geometric mean diameter (GMD) of the size fraction from 3 to 60 nm diameter and the effective deposition diameter. The GMD value (black line) was derived from the particle size distribution measurements. In the morning (08:00 CET), the GMD value drops from about 40 nm below 10 nm. This indicates elevated concentrations of nucleation mode particles, and thus, particle nucleation (Kulmala *et al.*, 2004). From 08:00 to 18:00 CET, continuous particle growth leading to GMD values between 30 and 50 nm can be observed.

The effective deposition diameter (grey diamonds) exhibits a similar diurnal pattern. Evidently, the onset of particle formation and the continuous growth behavior of the particle population between 08:00 and 18:00 CET is reflected in the D_{ed} data. The increased D_{ed} variation during nighttime (00:00 to 07:00, 20:00 to 24:00 CET) and between 12:00 and 14:00 CET is caused by poorly developed turbulence and thus reduced data quality.

In summary, the pattern of the effective deposition diameter clearly reflects the diurnal evolution of the particle size distribution, even though information about the actual size distribution is not used to derive this parameter. A comparison of the effective deposition diameter (D_{ed}) and the geometric mean diameter (GMD) of the particle size distribution reveals similar patterns of these two independent parameters. Thus, the GMD may be used as characteristic diameter of the particle population in order to estimate the total particle number flux. For this purpose, the particle deposition model is used to calculate the transfer velocity at the GMD, and the resulting transfer velocity is multiplied with the total particle concentration. In Fig. 7, the particle fluxes estimated (a) from the GMD and (b) from the summation of the

particle flux fractions of the individual size bins acc. to Eq. 3 are compared to the measured particle deposition fluxes obtained during the BEWA field campaigns 2001 and 2002.

→ Fig. 7

Evidently, both methods of estimation yield reasonable results. The scatter of the estimated flux values is similar in both cases. However, when estimated solely from the modeled transfer velocity of the GMD (Fig. 7a), the flux tends to be underestimated. This indicates that the large flux contribution of very small particles (large number and high transfer velocity) is underrepresented when the whole particle population is taken as a monodisperse population with the geometric mean diameter as the average particle size.

Another possible application of the new parameter is to use the effective deposition diameter to estimate the time evolution of the geometric mean diameter. From this information, the growth dynamics of the particle population can be derived. For example, constant particle growth rates are often observed during particle formation events and can be quantified through analysis of the GMD evolution (e.g. Held et al., 2004; Kulmala et al., 2004). The similarity of the GMD and D_{ed} patterns allows an estimation of particle growth rates from eddy covariance measurements in combination with a particle deposition model if measurements of the particle size distribution are not available.

4 CONCLUSIONS

The level of complexity that is required to describe the atmospheric turbulent exchange is lowered through the concept of the transfer velocity. The complex interactions of microphysical exchange processes are condensed in this single parameter. The integral transfer velocity is influenced both by the atmospheric turbulence regime and the ambient

particle size distribution. For a given turbulence regime, the integral transfer velocity of a nucleation mode dominated particle population will be larger than that of a population consisting mainly of accumulation mode particles with lower transfer velocities. Acc. to Eq. 4, the large number of nucleation mode particles with high transfer velocities will increase the integral transfer velocity.

Through analysis of directly measured integral transfer velocities, a comparison of the turbulent exchange behavior of particle populations at different sites and under different conditions is facilitated. In this study, the integral transfer velocities ranged from -37 mm s^{-1} to +23 mm s^{-1} with positive values (deposition) clearly dominating. Typical v_t values were on the order of 1 to 10 mm s^{-1} in accordance with similar studies at other coniferous forest sites (Buzorius *et al.*, 1998; Gallagher *et al.*, 2002). The modeled integral transfer velocities are on the same order of magnitude as the measured transfer velocities although they were overestimated in many cases. Thus, application of the model to study size-resolved particle deposition behavior was considered reasonable. Particle number fluxes are dominated by the abundance of ultrafine particles with high deposition velocities. Generally, the contribution of particles in the accumulation mode to the overall number flux is not significant. However, these particles constitute the submicron particle mass flux even though their transfer velocities are relatively low. Coarse particles with diameters > 1 µm were not in the focus of this work. These particles may exhibit large transfer velocities and consequently will dominate the overall mass flux. Due to their small numbers, eddy covariance measurements of number fluxes and calculation of mass fluxes as presented in this study is not reasonable for coarse particles.

The deposition model was used to determine the effective deposition diameter from particle flux measurements. Typically, the effective deposition diameter was below 200 nm. The 90 % percentile of 675 evaluations for the UCPC measurements was found at 191 nm, the median effective deposition diameter was 75 nm. These findings emphasize the dominance of

ultrafine particles in turbulent number fluxes (cf. Figs. 3a and 4). The similar patterns of the effective deposition diameter (D_{ed}) and the geometric mean diameter (GMD) of the particle size distribution were the motivation to use the GMD as a characteristic diameter of the particle population to estimate the total particle number flux. These flux estimates are comparable to the summation of the flux fractions derived from the size distribution measurements and the deposition model, and both estimates represent the measured fluxes reasonably well. In summary, these results indicate that for a detailed analysis of the size-dependence of turbulent particle exchange, direct measurements of size-resolved particle fluxes are urgently needed to evaluate and refine the theoretical models.

ACKNOWLEDGEMENTS

This work was funded by the German federal ministry of education and research (BMBF) through grants PT BEO 51-0339476 D (BITÖK) and PT UKF 07ATF25 (BEWA). We are grateful to J. Gerchau and G. Müller for their help during fieldwork. We also appreciate the support of the BEWA community.

REFERENCES

Birmili, W., Stratmann, F., and Wiedensohler, A. (1999) Design of a DMA-based size spectrometer for a large particle size range and stable operation. *J. Aerosol Sci.* **30**, 549-553.

Buzorius, G., Rannik, Ü., Mäkelä, J.M., Vesala, T., and Kulmala, M. (1998) Vertical aerosol particle fluxes measured by eddy covariance technique using condensational particle counter. *J. Aerosol Sci.* **29**, 157-171.

Buzorius, G., Rannik, Ü., Nilsson, E.D., Vesala, T., and Kulmala, M. (2003) Analysis of measurement techniques to determine dry deposition velocities of aerosol particles with diameters less than 100 nm. *J. Aerosol Sci.* **34**, 747-764.

Foken, T. (2003) Angewandte Meteorologie - Mikrometeorologische Methoden. Springer, Berlin, 289 pp.

Gallagher, M.W., Nemitz, E., Dorsey, J.R., Fowler, D., Sutton, M.A., Flynn, M., and Duyzer, J. (2002) Measurements and parameterizations of small aerosol deposition velocities to grassland, arable crops, and forest: Influence of surface roughness length on deposition. *J. Geophys. Res.* **107**, doi: 10.1029/2001JD000817.

Held, A., Nowak, A., Birmili, W., Wiedensohler, A., Forkel, R., and Klemm, O. (2004) Observations of particle formation and growth in a mountainous forest region in Central Europe. *J. Geophys. Res.,* **109**, D23204, doi:10.1029/2004JD005346.

Held, A. and Klemm, O. (2005) Direct measurement of turbulent particle exchange between a coniferous forest and the atmosphere. *submitted to Atmos. Environ.*

Klemm, O., Held, A., Kanter, H.-J., Mohnen, V., Hansel, A., Rappenglück, B., Sedello, C., Weitz, A., Steigner, D., and Steinbrecher, R. (2005) Experiments on forest/atmosphere exchange: Climatology and fluxes during two summer campaigns in NE Bavaria. *submitted to Atmos. Environ.*

Kulmala, M., Vehkamäki, H., Petäjä, T., Dal Maso, M., Lauri, A., Kerminen, V.-M., Birmili, W., and McMurry, P.H. (2004) Formation and growth rates of ultrafine atmospheric particles: a review of observations. *J. Aerosol Sci.* **35**, 143 – 176.

Matzner, E. (2004) Biogeochemistry of forested catchments in a changing environment: a German case study. Springer, Berlin, 498 pp.

Peters, K. and Eiden, R. (1992) Modelling the dry deposition velocity of aerosol particles to a spruce forest. *Atmos. Environ.* **26A**, 2555-2564.

Ruijgrok, W., Davidson, C.I., and Nicholson, K.W. (1995) Dry deposition of particles: Implications and recommendations for mapping of deposition over Europe. *Tellus* **47B**, 587-601.

Schwartz, S.E. (1996) The Whitehouse Effect – shortwave radiative forcing of climate by anthropogenic aerosols: an overview. *J. Aerosol Sci.* **27**, 359-382.

Seinfeld, J.H. and Pandis, S.N. (1998) Atmospheric chemistry and physics: from air pollution to climate change. John Wiley&Sons, New York, 1326 pp.

Slinn, W.G.N. (1982) Predictions for particle deposition to vegetative surfaces. *Atmos. Environ.* **16**, 1785-1794.

Steinbrecher, R., Rappenglück, B., Hansel, A., Graus, M., Klemm, O., Held, A., Wiedensohler, A., and Nowak, A. (2004) Vegetation-atmospheric interactions: The emissions of biogenic volatile organic compounds (BVOC) and their relevance to atmospheric particle dynamics. In: Matzner E. (Ed.) Biogeochemistry of forested catchments in a changing environment: a German case study. Springer, Berlin, 215-232.

TSI (1989) Model 3025 Ultrafine Condensation Particle Counter Instruction Manual Revision A, TSI Inc., St. Paul, MN, USA, 113 pp.

TSI (1998) Model 3760A/3762 Condensation Particle Counter Instruction Manual Revision B, TSI Inc., St. Paul, MN, USA, 82 pp.

Wallace, L. (2000) Correlations of personal exposure to particles with outdoor air measurements: a review of recent studies. *Aerosol Sci. Technol.* **32**, 15-25.

Wesely, M.L. and Hicks, B.B. (2000) A review of the current status of knowledge on dry deposition. *Atmos. Environ.* **34**, 2261-2282.

Zhang, L., Gong, S., Padro, J., and Barrie, L. (2001) A size-segregated particle dry deposition scheme for an atmospheric aerosol module. *Atmos. Environ.* **35**, 549-560.

TABLES

Tab. 1: Summary of parameters and values used in the particle deposition model (Zhang *et al.*, 2001). Adjustment of the empirical diffusion parameter to $\gamma = 0.81$ yielded the closest fit to 1:1 agreement between model results and measured data.

parameter	**symbol**	**unit**	**value**	**source**
particle density	ρ	$g\ m^{-3}$	1.3	see text
gravitational acceleration	g	$m\ s^{-2}$	9.81	Seinfeld and Pandis (1998)
dynamic viscosity at 20 °C	μ	$g\ m^{-1}\ s^{-1}$	$1.8\ 10^{-02}$	Seinfeld and Pandis (1998)
kinematic viscosity at 20 °C	ν	$m^2\ s^{-1}$	$1.5\ 10^{-05}$	Seinfeld and Pandis (1998)
mean free path of air	λ	m	$6.5\ 10^{-08}$	Seinfeld and Pandis (1998)
von-Kármán constant	κ	-	0.4	Foken (2003)
Boltzmann constant	k	$m^2\ g\ s^{-2}\ K^{-1}$	$1.381\ 10^{-20}$	Seinfeld and Pandis (1998)
empirical impaction factor	a_{im}	-	0.8	Peters and Eiden (1992)
empirical impaction factor	b_{im}	-	2	Peters and Eiden (1992)
reference height	z	m	10	estimate of aerodynamic height at site
roughness length	z_0	m	0.8	Zhang *et al.* (2001)
empirical diffusion parameter	γ	-	0.67 / 0.81	Slinn (1982) / this study
characteristic obstacle diameter	d_{obst}	m	$1.5\ 10^{-3}$	Peters and Eiden (1992)
empirical constant in surface resistance determination	ε_0	-	3	Zhang *et al.* (2001)

FIGURE CAPTIONS

Fig. 1

a) Modeled particle transfer velocity as a function of particle diameter, and b) measured particle size distribution in 40 size bins from 3 to 800 nm diameter on July 28, 2002, 12:00 – 12:30 CET.

Fig. 2

Measured (MEAS, black) and modeled (MOD, grey) integral transfer velocities from July 28 to 30, 2002.

Fig. 3

a) Modeled particle number flux, and b) modeled particle mass flux in 40 size bins from 3 to 800 nm diameter on July 28, 2002, 12:00 – 12:30 CET.

Fig. 4

Cumulative normalized concentration and flux of particle number and particle mass on July 28, 2002, 12:00 – 12:30 CET. Dashed lines indicate the particle fractions that contribute 95 % of particle number and mass flux, respectively.

Fig. 5

Modeled particle transfer velocity on August 02, 2001, 15:30 – 16:00 CET. The horizontal line corresponds to the measured integral transfer velocity v_{total}. Its intercept with the modeled transfer velocity indicates the effective deposition diameter D_{ed}.

Fig. 6

Geometric mean diameter in the size range from 3 to 60 nm diameter (GMD, black) and effective deposition diameter (D_{ed}, grey) on August 02, 2001.

Fig. 7: Comparison of measured particle fluxes with particle flux estimates derived a) from the transfer velocity at the geometrical mean diameter (GMD) and b) from the summation of flux fractions of the particle size distribution (PSD).

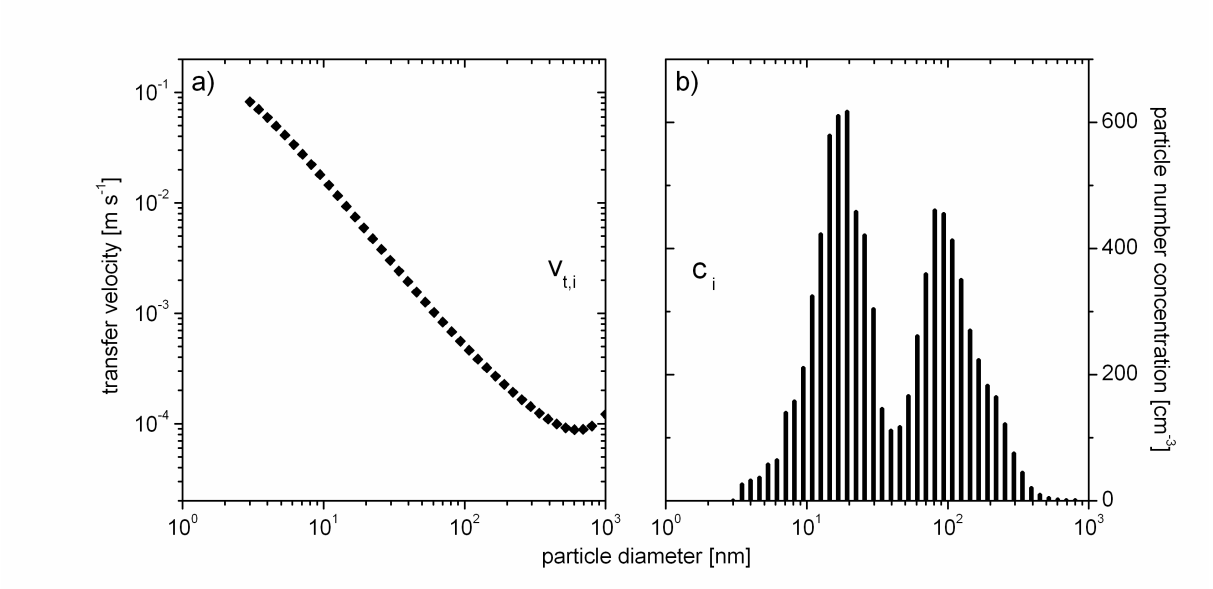
a)
b)
transfer velocity [m s-1]
particle number concentration [cm-3]
particle diameter [nm]
Vt,i
ci

Fig. 1

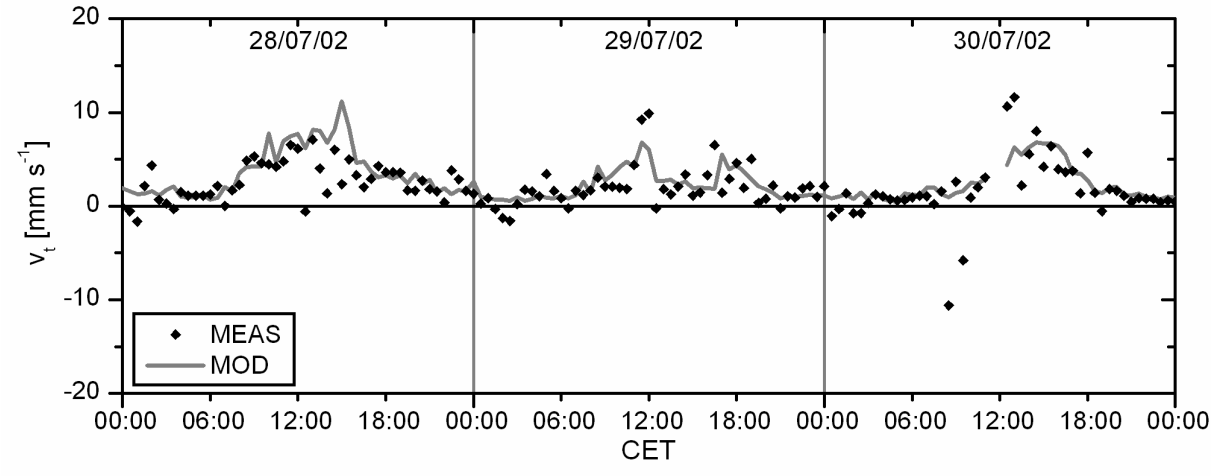
28/07/02
29/07/02
30/07/02
vt [mm s-1]
MEAS
MOD
CET

Fig. 2

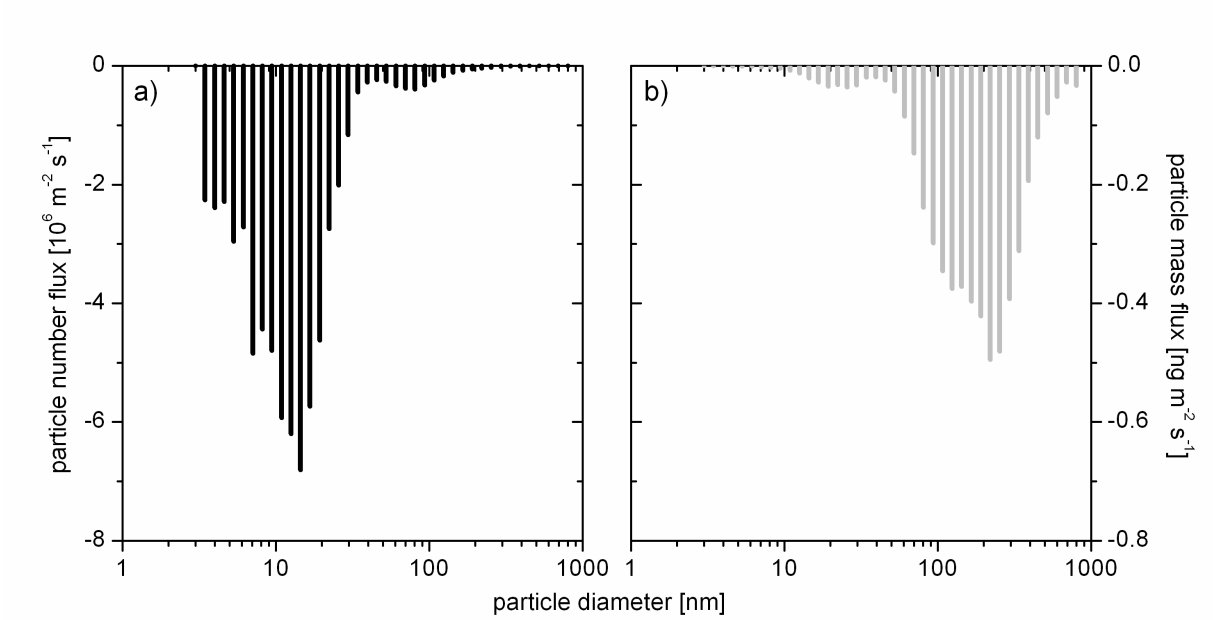
a)
b)
particle number flux [10^6 m^-2 s^-1]
particle mass flux [ng m^-2 s^-1]
particle diameter [nm]
0
-2
-4
-6
-8
0.0
-0.2
-0.4
-0.6
-0.8
1
10
100
1000

Fig. 3

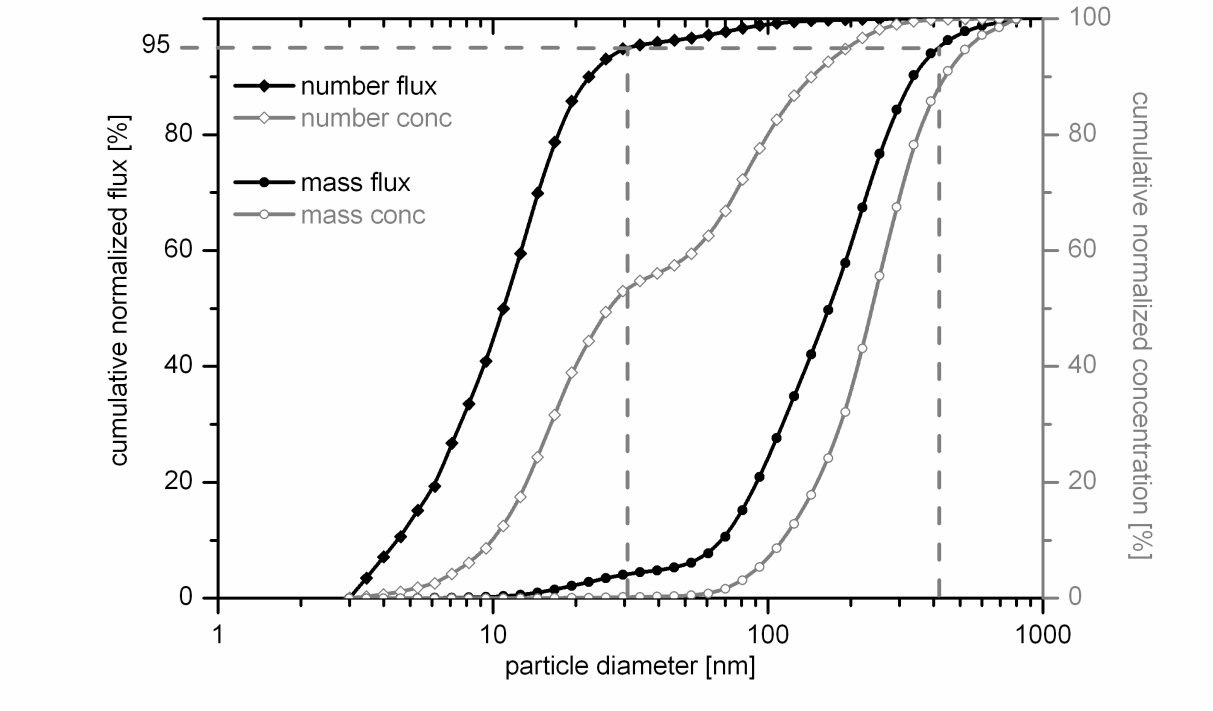
number flux
number conc
mass flux
mass conc
cumulative normalized flux [%]
cumulative normalized concentration [%]
particle diameter [nm]
95
80
60
40
20
0
100
1
10
100
1000

Fig. 4

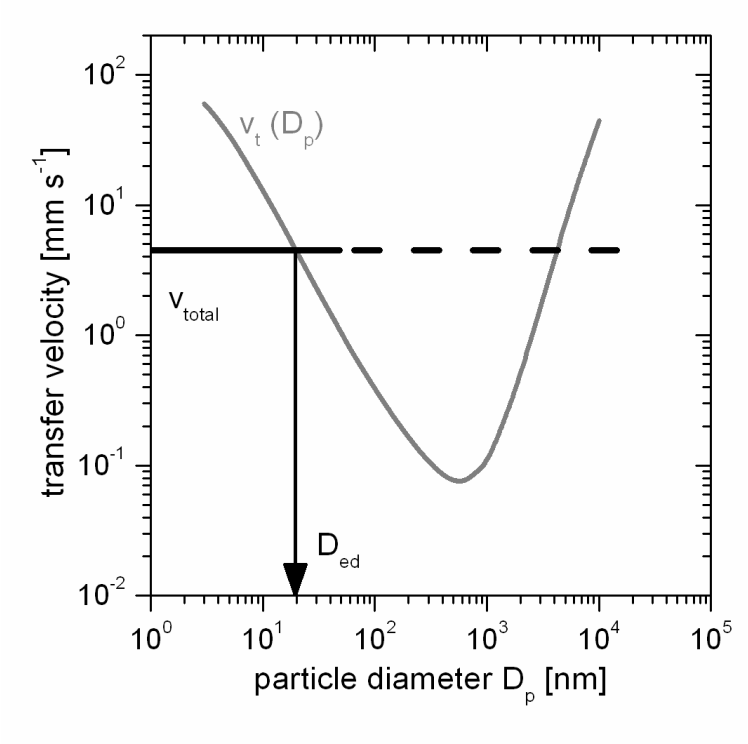
transfer velocity [mm s^{-1}]
particle diameter D_p [nm]
v_t (D_p)
v_{total}
D_{ed}

Fig. 5

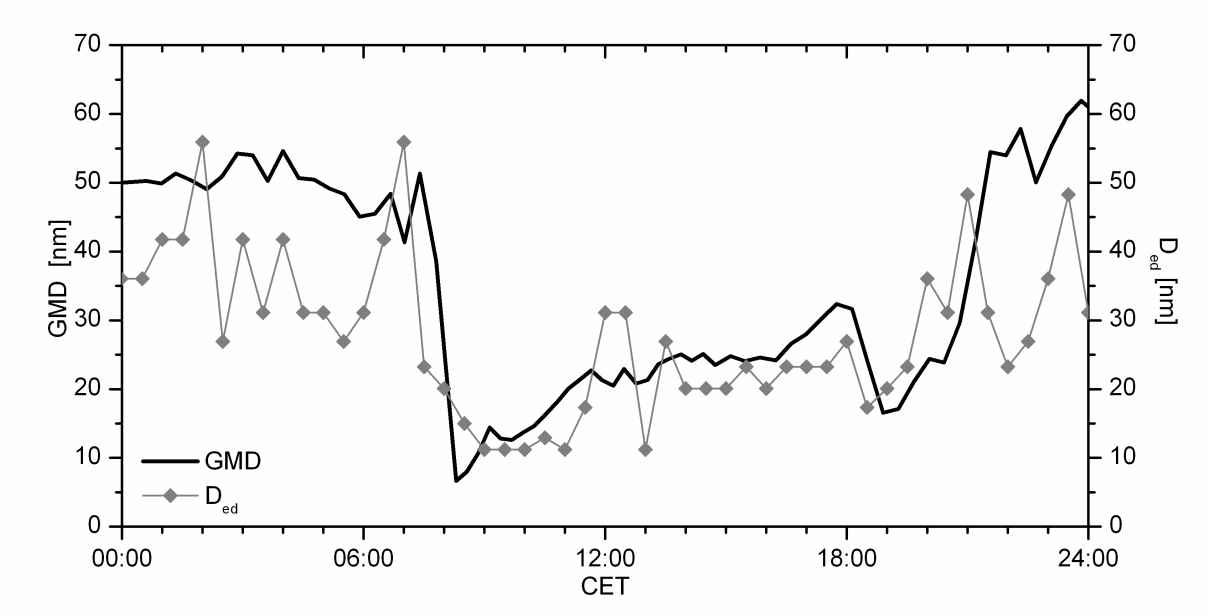
GMD [nm]
D_{ed} [nm]
GMD
D_{ed}
00:00
06:00
12:00
18:00
24:00
CET

Fig. 6

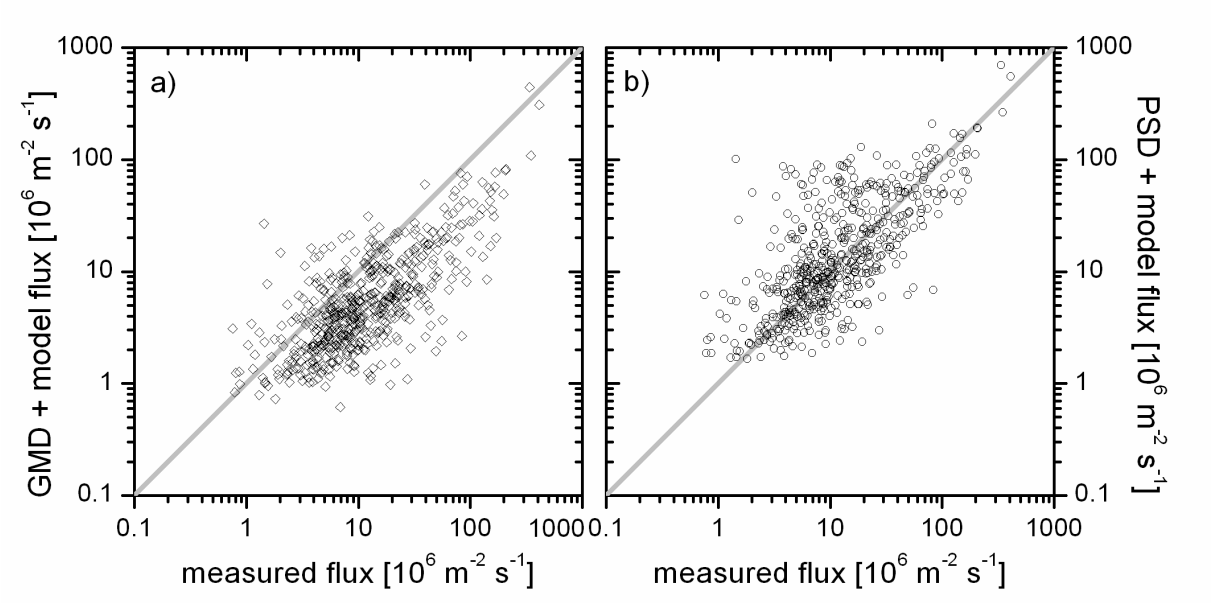
a)
b)
GMD + model flux [10^6 m^-2 s^-1]
PSD + model flux [10^6 m^-2 s^-1]
measured flux [10^6 m^-2 s^-1]
measured flux [10^6 m^-2 s^-1]
0.1
1
10
100
1000

Fig. 7